ACS APPLIED NANO MATERIALS

Article

High Spin Polarization in CoFeSn Heusler Nanowires for Spintronics

Ladislav Galdun, Pavol Szabó, Victor Vega, Enrique Diaz Barriga Castro, Raquel Mendoza-Reséndez, Carlos Luna, Jozef Kovac, Ondrej Milkovi#, Rastislav Varga, and Victor M. Prida

ACS Appl. Nano Mater., **Just Accepted Manuscript** • DOI: 10.1021/acsanm.0c01024 • Publication Date (Web): 22 Jul 2020

Just Accepted

High Spin Polarization in Co_2FeSn Heusler Nanowires for Spintronics

Ladislav Galdun*, Pavol Szabo, Victor Vega, Enrique D. Barriga-Castro, Raquel Mendoza-Reséndez, Carlos Luna, Jozef Kovac, Ondrej Milkovic, Rastislav Varga, Victor M. Prida*

Dr. L. Galdun*, Prof. R. Varga
CPM-TIP, UPJS,
Tr. SNP 1, 04011, Kosice, Slovakia.
*E-mail: ladislav.galdun@upjs.sk

Dr. P. Szabo, Dr. Jozef Kovac, Dr. O. Milkovic
Institute of Experimental Physics, Slovak Academy of Sciences,
Watsonova 47, 04001, Kosice, Slovakia

Dr. L. Galdun, Dr. V. Vega, Prof. V. M. Prida*
Departamento de Física, Facultad de Ciencias, Universidad de Oviedo,
C/ Federico Garcia Lorca nº 18, 33007, Oviedo, Asturias, Spain
*E-mail: vmpp@uniovi.es

Dr. E. D. Barriga-Castro
Centro de Investigación en Química Aplicada (CIQA),
Blvd. Enrique Reyna Hermosillo No.140, Saltillo, 25294, Coahuila, Mexico

Dr. R. Mendoza-Reséndez, Dr. C. Luna
Universidad Autónoma de Nuevo León (UANL), Av. Universidad S/N,
San Nicolás de los Garza, Nuevo León 66455, Mexico

Dr. O. Milkovic
Institute of Materials Research, Slovak Academy of Sciences,
Watsonova 47, 040 01 Kosice, Slovakia

ABSTRACT:

Cylindrical nanowires made of Co_2FeSn Heusler alloy with high spin polarization have been synthetized via template-assisted electrochemical deposition in nanoporous anodic alumina membranes. Their microstructure and morphology have been characterized by in situ studies of *X*-ray diffraction, together with scanning and transmission electron microscopy techniques. The basic structural and magnetic characterization revealed a B2-type cubic ordered Heusler structure with a lattice parameter of around 5.8 Å and the [110] direction, preferably aligned with the longitudinal axis of the polycrystalline nanowires. The easy magnetization axis is parallel to the nanowire´s axis too. The Point-Contact Andreev Reflection spectroscopic measurements performed on the nanowire´s fresh surface released high polarization values i.e., P = 0.85-1 and prove that the high spin polarization or half-metallicity will be preserved in the nanoscale regime. The presented results open the possibilities towards future exploration of Heusler nanowires with high spin polarization, which are promising materials for applications in spintronics and high-density magnetic data recording.

Keywords: Heusler alloys, electrodeposition, ferromagnetic nanowires, spin polarization, Spintronics

1. Introduction

The performance of conventional electronic devices can be significantly enhanced with spintronics, where not only the charge of the electron but also its spin is used to transfer and store the information.[1] Several Heusler alloys exhibit half-metallic nature, high Curie temperature, high magnetic moment, and low Gilbert damping, that makes them suitable candidates for spintronic applications.[2-5] The peculiar properties of Half-metallic materials arise from their electron density of states. While one of the spin channels behaves like an ordinary metal, the other one behaves as an insulator and exhibits an energy band gap at Fermi energy level.[3, 4] Therefore, Heusler alloys may enhance the performance of spintronic devices like magnetic tunnel junctions, giant magnetoresistance, or spin-transfer torque.[6, 7]

Previously, spin polarization values close to 100 % were observed for several materials, such as: EuS,[8] and EuO,[9] (both highly spin-polarized), Fe_3O_4,[10] and metastable CrO_2.[11] However, the mentioned materials are neither suitable for large spin transport effect nor compatible with applications or silicon platforms due to the poor electrical contact.[1, 2] Consequently, the search for novel materials with high spin polarization values continuously increases. Heusler alloys are another example of materials exhibiting excellent physical properties. Generally, Heusler alloys have X_2YZ stoichiometry and crystalize in $L2_1$ structure. In some cases, Heusler alloys may crystalize in disordered phases such as B2 (Y-Z disorder), DO_3 (X-Y disorder), or A2 (X-Y-Z disorder).[12, 13] Some of the disorders must be present, especially in the case of off-stoichiometric Heusler alloys. However, the influence of disorder on spin polarization in Heusler alloys is a complex task, since the spin polarization may be affected differently.

Sometimes the disorder may stabilize the half-metallicity, and in some cases, the presence of the disorder may reduce the spin polarization values.[13]

Thanks to the new experimental approaches, a significant evolution can be observed, especially in Heusler alloys, which are suitable for spintronic applications.[14] Heusler alloys have been widely studied in the form of bulk materials and thin films,[15-17] whereas the synthesis and study of these alloys in the form of 1D and 0D nanostructures remains an open challenge. The reduced size and the size- and shape-dependent properties of such nanostructures could preserve a disruptive role in diverse technological areas such as in spintronics, skyrmionic structures and topological insulators.[18]

Co_2-based Heusler alloys are well known for their high saturation magnetization and Curie temperature, which are the essential requirements for spintronic devices or magnetic-based memories.[19] Even though it is a hot topic, the fabrication of Co_2-based Heusler nanowires is not a trivial task, and only a few scientific papers are dealing with this issue.[20-29] The nanowires may exhibit strong perpendicular magnetic anisotropy for spintronics applications, but usually with the lack of spin polarization characterization.[30] There is still a strong demand for the preparation of next-level 3D magnetic "racetrack" memory devices. The racetracks are generally presented as magnetic arrays made of nanowires with a diameter of about 100 nm and few micrometers tall. One of the crucial parameters is the presence of the spin-polarized current that shifts the information written in the magnetic domain wall pattern with high efficiency.[31] Therefore we have decided to prepare Co_2-based nanowires with an even lower diameter (60 ±5 nm) as compared to our previous work (180 ±20 nm) and additionally determined the spin polarization.[26]

One of the biggest challenges for new materials that are considered for spin-injection is to determine their spin polarization ratio.[1] Therefore, the measurement of spin polarization in magnetic nanomaterials remains still as a difficult task. To the best of our knowledge, there are no experiments,

dealing with the direct experimental study of spin polarization in half-metallic nanowire arrays. Due to the limitation of optical methods on the nanoscale, electrical transport measurements are one of the simplest approaches for the determination of the spin polarization.[1] There is only one report on spin polarization measurements on $Fe_{1-x}Co_xSi$ nanowires, but with only the highest observed value of P = 0.35.[1] Here the question arises whether the half-metallicity is preserved in the nanoscale dimension.

The mentioned low spin polarization was obtained using a four-probe scheme with lithographically fabricated nanowire contacts.[1] On the other hand, classical point-contact Andreev reflection (PCAR) spectroscopy allows for the experimental study of spin polarization in a much simpler way, by measuring current-voltage (CV) characteristics on ballistic point-contacts formed by pressing a sharp superconducting tip to the surface of a spin polarized system.[1, 15, 32-34]

Co_2FeSn Heusler alloy is a suitable candidate from the Co_2-based group because of the predicted high spin polarization values.[35] It has also been shown earlier that the deposition of Co_2FeSn Heusler alloy from aqueous solution in the form of thin films and nanowires is possible.[36-38] Therefore, Co_2FeSn alloy nanowires have been grown in the nanopores of Anodic Alumina Oxide (AAO) membrane using the pulsed electrochemical deposition method (Figure 1). The presented approach can be used to fabricate new Heusler nanowires with high spin polarization for spintronic applications.[26] Moreover, it allows the fast production of a large amount of uniform ferromagnetic nanowires formed in dense arrays. To determine the spin polarization values of prepared nanowires, we have performed PCAR spectroscopy measurement using mechanically formed ballistic point-contacts between the array of Co_2FeSn nanowires and the superconducting Nb tip. It is shown that by creating a contact with a fresh surface of the nanowires in the array it is possible to obtain very high spin polarization values.

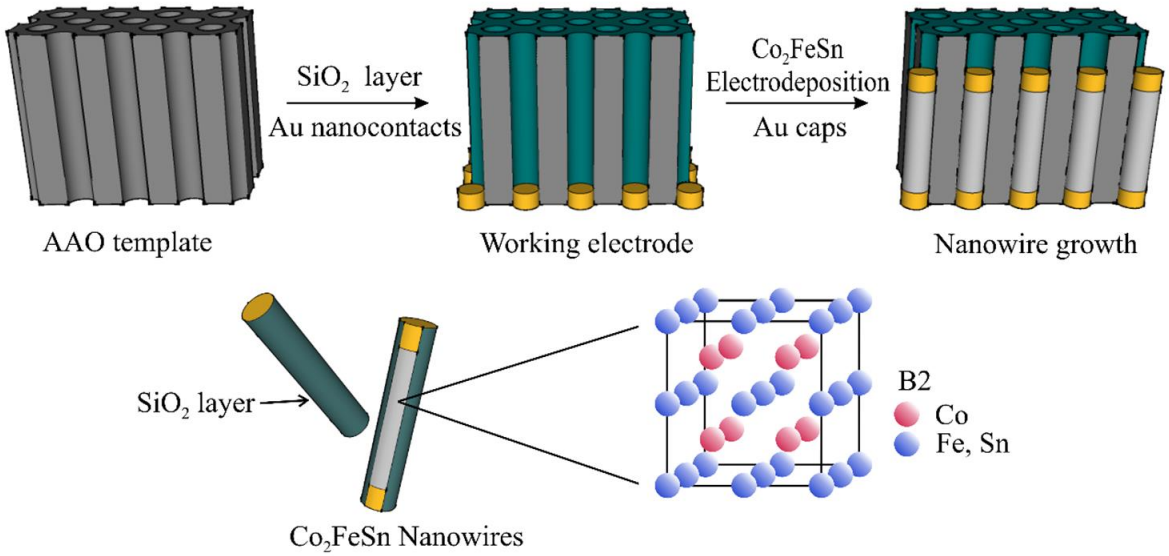

Figure 1. Schematic representation of Co_2FeSn nanowires synthesis method based on AAO template-assisted electrodeposition. The nanowires are covered with a protective SiO_2 layer deposited by ALD, and they can be easily released from the AAO membrane by selective chemical etching.

2. Results and Discussion

2.1. Microstructure and compositional analysis of Heusler nanowires

The shape, chemical composition, and crystalline structure of the Co_2FeSn nanowires were characterized by transmission, scanning, and scanning transmission electron microscopy techniques (TEM, SEM and STEM, respectively), and energy dispersive X-ray spectrometry (EDS). Figure 2 (left) shows the cross-section of the AAO membrane filled with deposited Co_2FeSn nanowires (60 (±5) nm diameter, 10 μm long) and having about 105 nm of internanowires spacing distance. The gold nanocontacts and the additional Au segments on the top of the nanowires may be well recognized as well. The thickness of the protective SiO_2 coating layer deposited by atomic layer deposition (ALD) technique is about 4 nm. EDS elemental mapping studies show a rather uniform distribution of the Co, Fe and Sn elements along the entire nanowires (Figure 2 (right, down)). The quantification of the atomic composition of the Co-Fe-Sn

alloyed nanowires obtained from the EDS measurements indicates the following atomic contents: 53 (±2) at% of Co, 20 (±2) at% of Fe, and 27 (±2) at% of Sn.

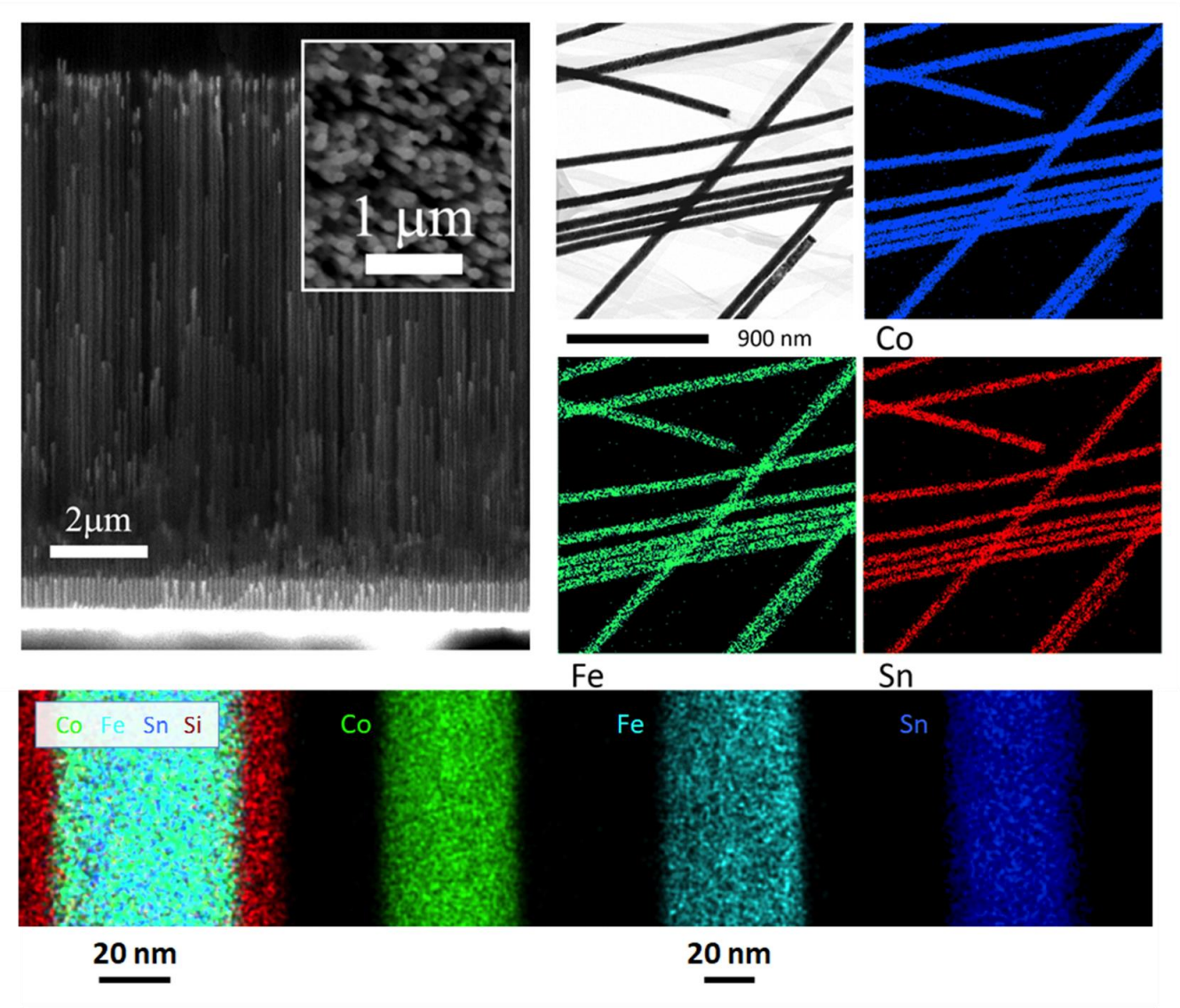

Figure 2. (left) the corresponding cross-section for the Co_2FeSn nanowires in the array and SEM micrograph of the top view of free-standing nanowires without upper Au caps and protective SiO_2 coating layer which is not present in the case of the sample prepared for microcontact spectroscopy (inset). (right, down) STEM analyses of Co_2FeSn nanowires with EDS mapping disclose the uniform distribution of the atomic content of Co, Fe and Sn into the nanowires and the presence of the SiO_2 coating layer.

X-ray diffraction (XRD) pattern (Figure 3a) of self-assembled Co_2FeSn nanowires electrodeposited into the alumina template, measured at room temperature, displays an intense peak at 44.25º and a very small peak at around 30°, which are assigned to the (220) and (200) reflections, respectively, of the body-centered cubic (bcc) Co_2FeSn Heusler structure with a lattice parameter of 5.784 (±4) Å, in agreement with the previous studies.[38] Other reflections are not observed in this pattern. This fact and the large difference between the intensities of the (200) and (220) diffraction peaks indicate that the nanowires exhibit a crystalline texture with the [110] direction preferentially oriented along the nanowire axis. The obtained value of the mean coherence length, L_{220} = 10 nm, is significantly smaller than the length and width of the nanowires, indicating that the nanowires are polycrystalline and formed by several nanocrystals that tend to share their [110] direction oriented along the long nanowire axis.

Microstructural analysis using high resolution (HR) and dark-field TEM images in combination with Selected Area Electron Diffraction (SAED) measurements (Figures 3b-3e), confirm the polycrystalline character of the nanowires and their B2 cubic crystalline structure. Fig. 3b is a SAED pattern of several nanowires that may be indexed to the reflections of the (200), (220), (400), (422), (440), and (620), which are characteristic for a pure cubic B2 Heusler structure.[39] This structure is defined with the Y-Z (Fe-Sn) disorder, and according to theoretical calculation this fact may result in a slight reduction of the spin polarization values.[40] Figure 3c shows a dark-field TEM image of a single nanowire where several nanocrystals are distinguished. The study of a small area of a single Co_2FeSn Heusler nanowire by HRTEM (Figure 3d) and SAED (Figure 3e) shows that the B2 Heusler nanocrystals of the nanowires roughly tend to display their [110] direction along the long nanowire axis in agreement with the conclusions obtained from the XRD analysis.

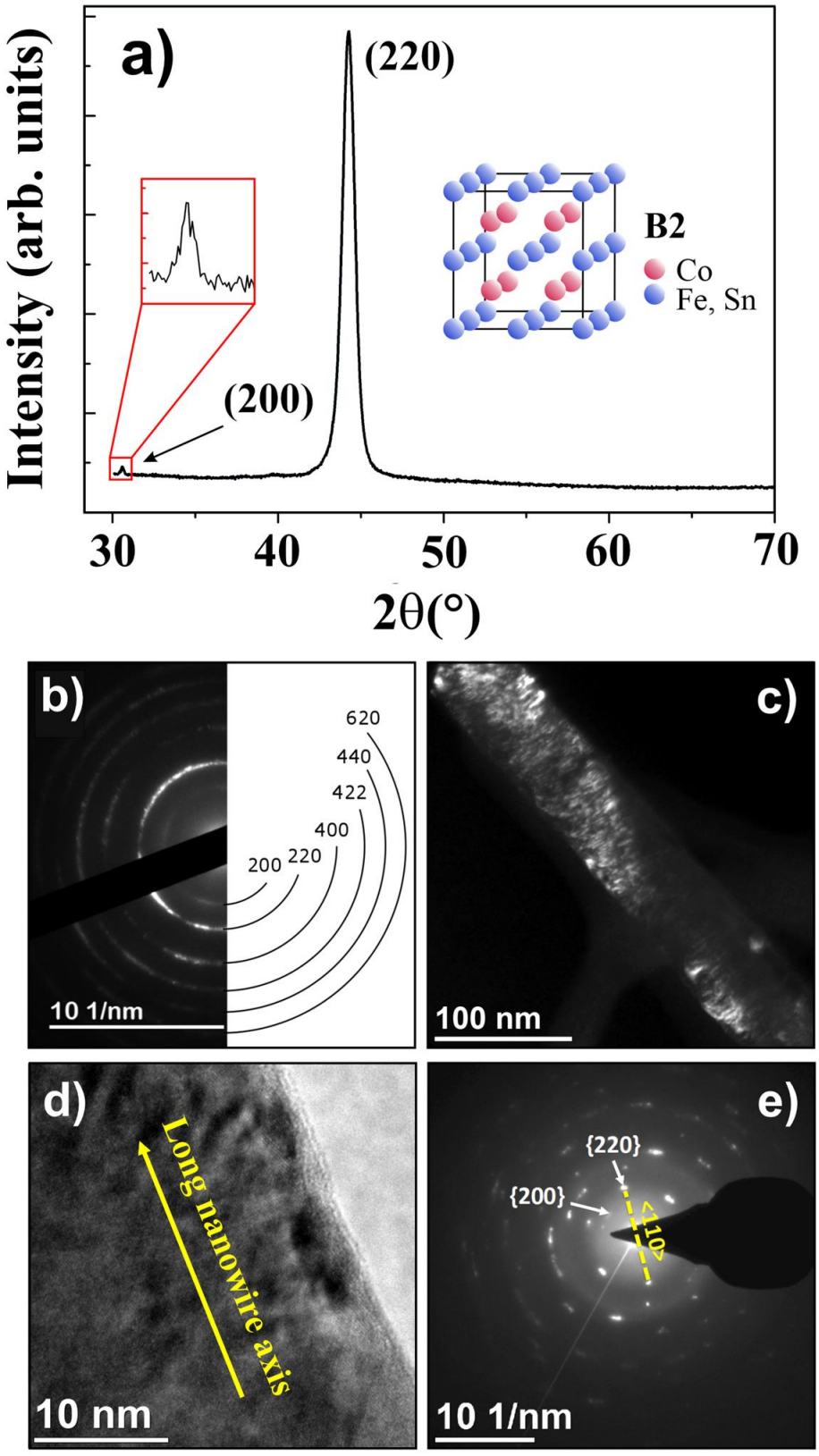
a)
(220)
(200)
B2
Co
Fe, Sn
Intensity (arb. units)
30
40
50
60
70
2θ(°)
b)
620
440
422
400
200
220
10 1/nm
c)
100 nm
d)
Long nanowire axis
10 nm
e)
{220}
{200}
<110>
10 1/nm

Figure 3. (a) XRD pattern of Co_2FeSn nanowires electrodeposited into the alumina template with B2 cubic phase, (b) SAED pattern corresponding of several nanowires indexed to the B2-type cubic Co_2FeSn Heusler structure. (c) Dark-field TEM image of a single nanowire. (d) HR-TEM micrograph of a single Co_2FeSn nanowire, the arrow indicates the direction of the long axis of the nanowire, (e) SAED pattern of the same area studied in the panel (d). It is observed that the direction of the long nanowire axis, highlighted in panel (d), roughly falls in the <110> direction (see panel (e)).

2.2. Magnetic properties and Spin Polarization of Co_2FeSn nanowires

The magnetic properties of Co_2FeSn Heusler nanowires located in the AAO membrane have been determined with the magnetic hysteresis loop measurements. The sample has been measured in the magnetic field with the parallel and perpendicular orientation to determine the nanowire´s easy magnetization axis, at the temperature of 300 K (Figure 4a). The bulk hysteresis loops of the NW array reveal their soft magnetic behavior with a saturation magnetization of about 1657 emu/cm^3 and low coercive field (H_C) values. It can be seen (inset of Figure 4) that the coercivity measured in the parallel direction reaches higher values (~360 Oe) than in the perpendicular direction (~17 Oe). This indicates that the easy magnetization axis is parallel to the nanowires axis due to the shape anisotropy.

In both parallel and perpendicular directions, the magnetization saturation of the nanowires arrays is reached in the high magnetic field range via magnetization rotation process. The presence of strong magnetostatic interactions between the nearest neighboring nanowires leads to the poor squareness and narrow coercive field.[26, 41-43] This effect results in a subsequent switching of individual nanowires even though the nanowires exhibit similar coercive fields and good squareness, as observed in our previous study.[26] Additionally, the temperature dependence of magnetization confirmed high Curie temperature well above 1000 K, as shown in Figure 4b. On the other hand, in the case of magnetic racetrack memory

the huge anisotropy is not necessary, the squareness of a single domain (bit) is almost 100%, and the coercivity can be enhanced with the pinning centers.[44]

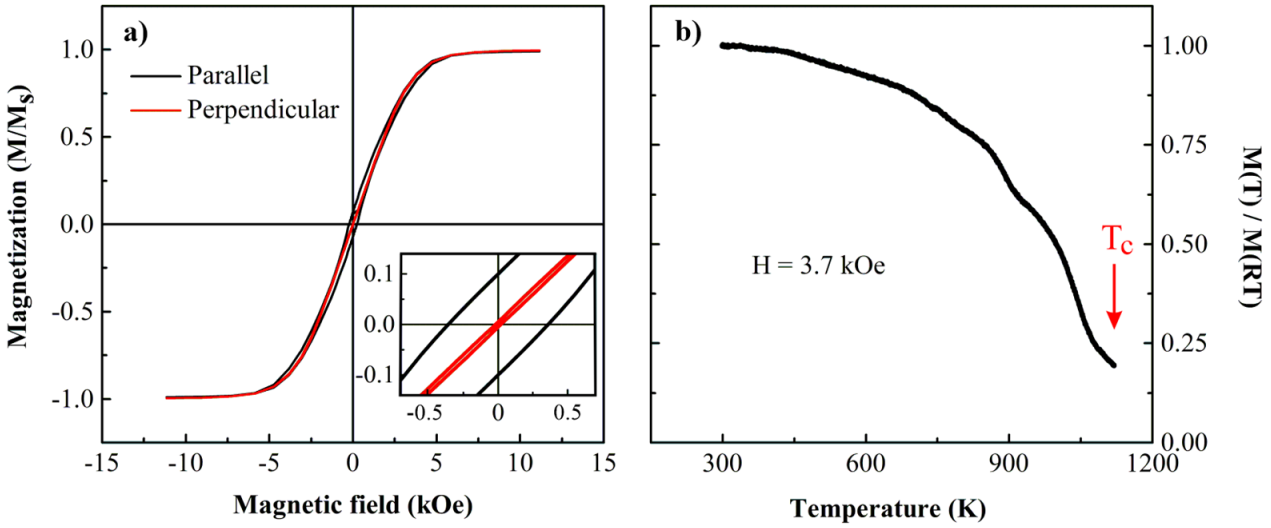

Figure 4. (a) Magnetic hysteresis loops measured at 300 K in an array of Co_2FeSn nanowires for both the parallel and perpendicular direction with respect to the nanowire´s axis, (b) normalized temperature dependence of magnetization M(T)/M(RT), revealing high Curie temperature (>1000 K).

The spin polarization of the Co_2FeSn nanowire arrays was studied by means of PCAR spectroscopy measurements.[15, 32, 45, 46] This method enables direct experimental study of the superconducting energy gap through point-contacts formed between a normal metal (N) and a superconductor (S).[32] The spectroscopy conditions are fulfilled only in ballistic contacts, where the dimension of the microconstriction is smaller than the mean free path of electrons. The PCAR conductance measured on N-S ballistic point-contacts can be described with the Blonder-Tinkham-Klapwijk (BTK) theory.[45, 46] This theory, introducing parameters of the superconducting energy gap Δ, the barrier strength Z and the spectral broadening Γ (which is the imaginary part of the energy [15, 45] $E = E' + i\Gamma$), explains the evolution of the PCAR spectra between a pure metallic ($Z = 0$) and a tunneling like

($Z >> 0$) point-contact. At low temperatures $T \rightarrow 0$ and high contact transparency $Z = 0$, the Cooper pairs are injected at the PC interface at energies $E < \Delta$ through Andreev reflection. Accordingly, the PC conductance doubles at energies inside the gap. The increase of the barrier strength Z reduces the PC conductance around zero energy forming two well-defined peaks at $\pm \Delta$. It is important to notice, that only non-polarized electrons can take a part at the Andreev scattering processes.

When a ballistic point-contact is formed between a superconductor and a metal with the degree of spin polarisation, the Andreev reflection contribution is reduced with the level of spin polarisation.[32] The transport of charge carriers through such point-contact can be described with the BTK model modified for the Andreev-reflection of quasiparticles in spin-polarized systems (MBTK). This two-channel model defines the PCAR conductance as the weighted sum of the Andreev-reflection and the spin-polarized channel contribution. [11, 15, 45, 47] The value of P is then defined through the weight of the spin-polarized channel.[15]

Our experiments were performed on Nb/NW array point-contacts. Due to the direct contact of the Nb tip with several Co_2FeSn nanowires, multiple ballistic contacts offered ideal conditions for PCAR measurements. There will be no difference between PCAR spectra measured on one or more nanowires. All parameters determined from fitting procedure represent the average value of the multiple ballistic contact. Tens of point-contact spectra were measured on different areas of NW array at $T \sim 1.5$ K. The ballistic PCAR spectra with a characteristic superconducting gap structure were measured at contact resistances in the range $R_{PC} = 5 – 35\ \Omega$. The spin polarization parameter P was determined from fitting of the PCAR spectra to the thermally smeared MBTK model. The fitting procedure employed a constant value $\Delta_{Nb}(0) = 1.53$ meV, so the Andreev reflection contribution was controlled mainly through the parameters P, Z and Γ. The suppression of spectral features with increased Γ had to be excluded because its strongly enhanced value shifts the gap maxima positions to higher energies and the gap $\Delta_{Nb}(0) = 1.53$ meV cannot fit the suppressed Andreev reflection contribution. The values of P were determined

exclusively from PCAR spectra measured on highly transparent contacts (Z<0.5).[11, 15 46, 47] The correctness of the fitting procedure was verified with fitting of the temperature dependence of the PCAR spectra from the lowest experimental temperatures up to the critical temperature of the superconducting state of niobium. When the value of P is determined correctly, the whole temperature dependence can be fitted with the same values of P, Z, Γ and the only temperature-dependent parameter Δ reveals BCS-like temperature dependence.[32]

Figure 5 shows the temperature dependence of the Nb/NW array point-contact spectra (solid gray lines). The solid lines represent the fitting curves, which have been obtained at almost temperature-independent values of the fitting parameters P = 0.65, Z = 0.34, Γ = 0.16 ± 0.2 meV. The only temperature dependent parameter, the energy gap $\Delta(T)$ is plotted with black symbols in the inset of Figure 5. It is evident, that the suppression of the gap with increased temperature follows the predictions of the BCS theory (solid line). The obtained BCS-like temperature dependence of the energy gap of niobium with $\Delta_{Nb}(0)$ = 1.53 meV and the almost temperature-independent values of the fitting parameters P, Z and Γ strongly support the correctness of the fitting procedure.

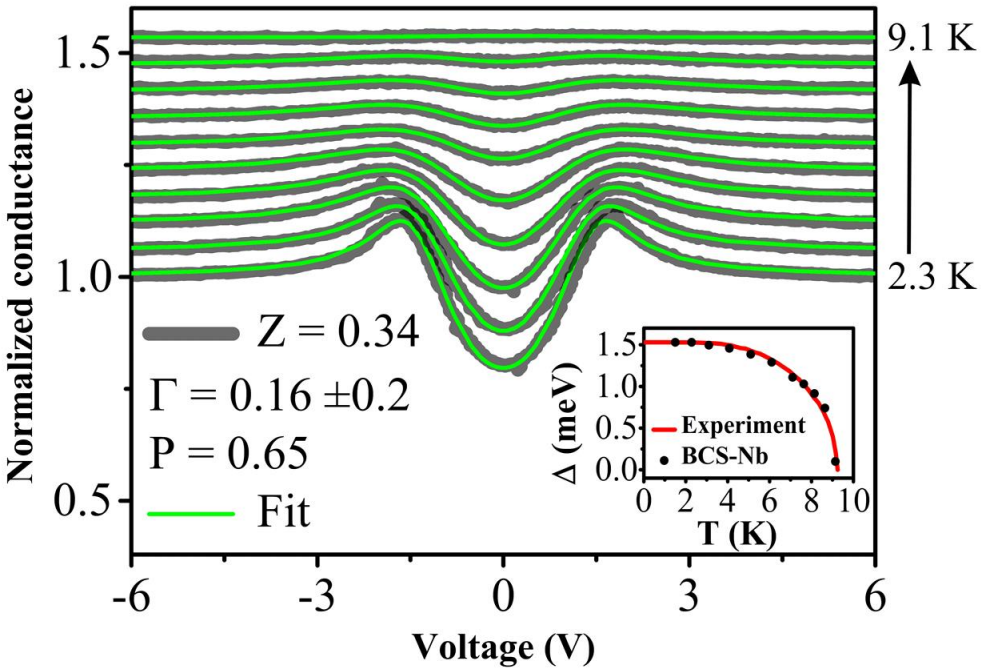

Figure 5. Temperature dependence of the Point-Contact Andreev Reflection spectra measured on an Nb/NW array point-contact at temperatures from the bottom curve 2.3 K, 3.1 K, 4.1 K, 5.1 K, 6.1 K, 7.1 K, 8.1 K, 8.6 K, and 9.1 K (gray symbols) and the corresponding fitting curves (green lines) and fitting parameters (see the legend). The inset shows the evolution of the superconducting energy gap of the Nb tip with temperature (black symbols) and predictions of the BCS theory (red line).

The left panel of Figure 6 depicts typical PCAR spectra measured on Nb/NW array point-contacts at T = 1.5 K with symbols, where the solid green lines are fitting curves. The corresponding fitting parameters P and Z are shown in the legends. The smearing parameter Γ was in the range $\Gamma \sim 0.1\Delta$-0.5Δ. PCAR spectra measured through point-contacts formed with weakly (weak PC) and strongly pressed Nb tip (strong PC) to the natural surface of NW array are shown in the bottom and middle panel, respectively. The upper panel shows the spectra measured on freshly cleaved surfaces of the Heusler nanowires (fresh point-contacts). The cleavage (breaking of nanowires) was performed in-situ with a horizontal movement of the strongly pressed Nb tip. Our main result, concerning the evolution of the spin polarization parameter P with the point-contact barrier strength Z determined from the fitting of all measured PCAR spectra at the lowest experimental temperatures, is displayed in the right panel of Figure 6.

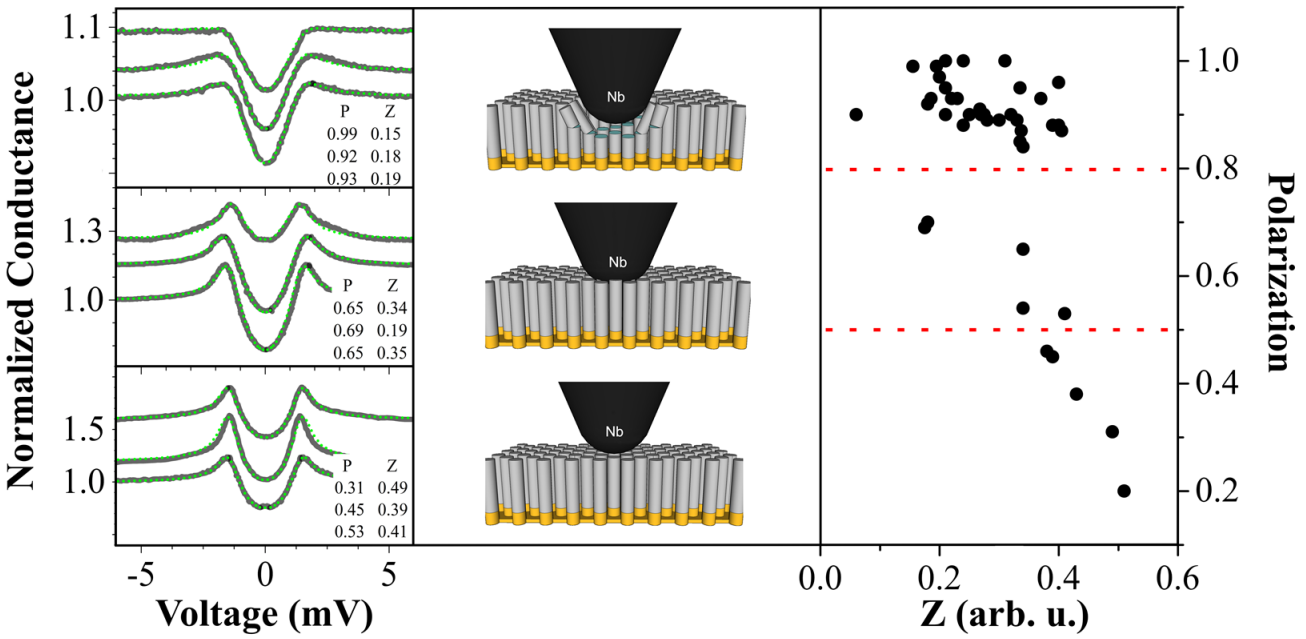

Figure 6. Spin polarization (*P*) dependence on barrier strength (*Z*) for Co_2FeSn nanowire arrays - right panels and examples of PCAR experimental data (gray lines) and fits (green symbols) at T = 1.5 K in three different measuring modes – left panels. The values of spectral smearing parameter Γ were between $\Gamma \sim 0.1\Delta$-0.5Δ. The results shown in the bottom and middle panels are characteristic for the point-contacts formed with weakly and strongly pressed Nb tip to NW array, respectively. The upper panels show results obtained on freshly cleaved NW array surfaces. The central 3D pictures visualize the point contact area in each mode.

Comparing the experimental conditions (depicted in 3D drawings in Figure 6) with the obtained *P*-*Z* dependence, important surface properties of our Co_2FeSn nanowires can be found. The very first "weak PCs" measured on different areas of the NW array sample show the lowest point-contact transparency and the lowest values of the spin polarization parameter. When the Nb tip was weakly pressed into the NW array surface, we observed a decrease of the contact resistance from 35 Ω to 25 Ω, a reduction of the barrier strength Z from 0.5 to 0.4 and an evident increase of the spin polarization parameter *P* from 0.2 to 0.5 (lower panels in Fig. 5). It indicates the presence of surface phase(s) or

material deterioration with lower spin polarization compared to the inner part of the nanowires. Surface oxidation can occur during the chemical etching of the alumina membrane. Therefore, we tried to suppress the influence of surface effects or oxides by pressing the Nb tip deeper into the surface of nanowires. We were able to reduce the point-contact resistance down to $R \rightarrow 10\ \Omega$ and the barrier strength parameter to $Z \rightarrow 0.2$, keeping the ballisticity of the contacts. The possible partial cleaning of the surfaces enabled us to see deeper into the sample and approach the phase(s) with polarization $P \rightarrow 0.8$ (Figure 6, middle panels).

The highest values of the spin polarization were observed on "fresh PCs" (top panels in Figure 6). In these contacts, the spin polarization *P* is not a function of the barrier strength *Z*. The values are scattered in the range $P = 0.85–1$ in the broad interval of the barrier strength $Z = 0.1\text{-}0.4$. It means that, due to the *in situ* cleaving, the influence of the oxidized surface layer is missing. The obtained *P* values represent the average of the spin polarization of each nanowire forming the point-contact. It suggests, that, the very high spin polarization *P* is an inherent property of the Co_2FeSn nanowires. These values of the spin polarization are much higher than in the case of Co_2FeSn layers studied in a sandwich of Fe/MgO/Co_2FeSn magnetic tunnel junctions (MTJ).[48] Moreover, the obtained values are even higher than in the case of PCAR measurements performed on Heusler alloys with similar composition.[33, 34, 49, 50] We suppose that the high values of spin polarization observed in our experiments on Co_2FeSn nanowires are connected with the unique presented experimental approach.

A dense array of parallel nanowires protruding from a conducting substrate enabled *in situ* cleaving and forming ballistic point-contacts for a direct experimental study of spin polarization on extremely clean surfaces of Co_2FeSn nanowires. When the cleavage is made carefully, the broken parts of the nanowires will not cover the full contact area, and the point-contact current will flow through the areas with the lowest resistances (cleaved surfaces of nanowires in the NW array).

3. Conclusions

In conclusion, Co_2FeSn Heusler alloy nanowires having a mean diameter of 50 nm, 105 nm of internanowires distance, and around 10 μm in length have been grown in nanoporous AAO membranes using potentiostatic pulsed electrochemical deposition. Structural XRD, HR-TEM and SAED, together compositional EDS analysis and basic SQUID magnetic characterization confirmed uniform chemical distribution of the elements and the polycrystalline character of Co_2FeSn nanowires having a B2-type cubic ordered Heusler structure, with a lattice parameter of 5.784 (±4) Å that displays the grain [110] direction preferably aligned with the longitudinal axis of the nanowires. The basic magnetic characterization carried out on the Co_2FeSn nanowires array supports their soft magnetic character having a saturation magnetization of about 1657 emu/cm^3 and with their easy magnetization axis lying along the nanowire´s longitudinal direction. The spin polarization measurements were performed by using the Point-Contact Andreev Reflection spectroscopy, where a superconducting Nb tip was used to make the point-contact with the surface of the free-standing nanowires. After the mechanical cleavage of the Heusler nanowires in the array, the PCAR measurement revealed high spin polarization values in the range of P = 0.85-1 %. We show that the high spin polarization values or even the half-metallicity is preserved in the nanoscale regime, and the presented approach enables the direct experimental study of spin polarization on extremely clean, freshly cleaved surfaces. Therefore, the presented template-based synthesis method offers an easy approach for producing a considerable amount of uniformly arranged nanowires with novel chemical composition. Such architecture made of spin-polarized Heusler based alloy with high spin polarization is suitable for the future 3D “racetrack” memory, enhancing the capacity of solid-state magnetic data storage devices. Moreover, with the reduction of the pore diameters it is possible to prepare nanowires with lower diameter (10-15 nm) and therefore significantly enhance the density of the nanowires and possible data storage capacity.

4. Experimental Section

Synthesis of Co_2FeSn Heusler alloy nanowires: In the present work, the Co_2FeSn nanowires were electrochemically deposited from the aqueous electrolyte, which contained metallic (Co, Fe, Sn) salts and different additives. To be able to perform the synthesis of Co_2FeSn nanowires, (Figure 1), the backside of a SiO_2 modified AAO template was firstly coated with a gold layer using Au sputtering (Polaron SC 7620). In the next step, Au nanocontacts with a length of about 1 μm, have been potentiostatically deposited from a gold plating solution Orosene 999.[26] The Au nanocontacts can be distinguished in the light gray bottom part of the scanning electron micrograph of Figure 2. Subsequently, the deposition of Co_2FeSn nanowires was performed from the aqueous solution (*pH* = 1.4) containing: Cobalt chloride (0.16 M), Iron sulfate (0.072 M) and Tin chloride (0.243 M), Sodium chloride (0.34 M), Gelatin (0.1 g/l) Saccharin (1 g/l) and Ascorbic acid (1 g/l). The acidic *pH* value of the electrolyte was carefully optimized to avoid precipitation of Sn. At the same time, gelatin enhances nucleation and minimizes dendritic growth, thus allowing the creation of complete Co_2FeSn nanowires with a smooth surface, analogously to the case of Sn coatings.[51]

The Co_2FeSn nanowires synthesis was performed by potentiostatic pulsed electrodeposition (PED). The electrochemical set up consisted of a Teflon cell, a counter electrode (Pt wire mesh), a working electrode (AAO template with the gold coating), and a reference electrode (Ag/AgCl). The PED mode consists of pulses of 1.3 V (vs. reference electrode) and break pulses (open circuit potential). Each pulse was applied for 1 s. After about 30 minutes, the nanowires with approximately 10 μm in length were grown. The nanowires were released from the AAO membrane for transmission electron microscopy (TEM), by using chemical etching. Therefore, protective Au caps (0.4 μm) were deposited on the top side of the nanowires (Figure 2).[26] The sample for spin polarization measurement was prepared without the SiO_2 layer and protective Au caps on the free side of the nanowires. After the electrodeposition of

the nanowires, the AAO membrane was completely removed by selective chemical etching using 3M NaOH. After this modification, the dense NW array is suitable for point-contact spectroscopy. The bottom (golden) side of the sample was supported with additional Cu electrodeposited layer to enable electrical contacting of each nanowire in the array and avoid the destruction of the NW array sample.

Microstructural and compositional characterization: A PANalytical X´Pert Pro MPD diffractometer, equipped with an Anton Paar HTK 1200N oven furnace and with Cu *Kα* radiation (λ=1.540598 Å), was employed to measure the X-ray diffraction (XRD) patterns of samples at room temperature. The scattering angles 2θ was varied in the range from 30º to 90º with a scan step size of 0.0394º. The mean coherence length along the [220] direction, L_{220}, of the body-centered cubic (bcc) Co_2FeSn Heusler phase was determined using the Scherrer formula:[52]

$$L_{220} = \frac{0.9\lambda}{(\beta \cos\theta)} \quad \textbf{(1)}$$

where λ is the x-ray wavelength, β is the broadening of the (220) peak of a bcc phase and θ is the Bragg angle.

The morphology and compositional analysis of the NW array were performed on Scanning electron microscope (SEM), JEOL-6100 with an accelerating voltage of 20 kV.

A FEI-TITAN 80-300 kV microscope was operated at 300 kV to collect transmission electron microscopy (TEM) images and selected area electron diffraction (SAED) patterns at room temperature. Scanning transmission electron microscopy (STEM) characterizations were carried out with the same microscope in high-angle annular dark-field (HAADF) mode. Energy dispersive X-ray spectroscopy (EDS) compositional mapping studies were also realized during the TEM and STEM measurements to determine the chemical composition with higher precision.

Magnetic properties and spin polarization measurements: The magnetic characterization of the NW array was performed using the Magnetic Property Measuring System (MPMS) with a

Superconducting QUantum Interference Device (SQUID), Quantum Design. The hysteresis loops were measured under applied magnetic field up to 50 kOe and in the temperature range from 10 to 400 K.

The temperature dependence of magnetization has been measured with an in-house-made VSM apparatus in the external applied magnetic field of 3.7 kOe.

PCAR measurements have been performed in a home-made point-contact spectroscopy insert with a mechanical X-Z approaching system enabling measurements in the temperature range T = 1.5 – 300 K in magnetic fields up to B = 8 T.[15, 32, 44, 46] The point-contacts have been performed on different surface areas at T = 1.5 K with a sequential pressing of a sharp superconducting Nb tip to the natural or freshly cleaved surface of the studied NW array samples (Nb/ NW array point-contacts). The cleavage has been performed in-situ below T < 4.2 K with a horizontal movement of the strongly pressed Nb tip. The differential conductance has been measured using a standard lock-in technique.

Acknowledgements

This research was supported by Slovak Grant Agency VEGA 1/0053/19, Slovak Grant Agency grant number APVV-16-0079 and VVGS-2019-1231. Spanish MICINN under research grants Nº MAT2016-76824-C3-3-R and PID2019-108075RB-C32 are also acknowledged. Scientific support of common research services of SCTs from Universidad de Oviedo is also gratefully recognized.

References

(1) DeGrave, J. P.; Schmitt, A. L.; Selinsky, R. S.; Higgins, J. M.; Keavney, D. J.; Jin, S. Spin Polarization Measurement of Homogeneously Doped $Fe_{1-x}Co_xSi$ Nanowires by Andreev Reflection Spectroscopy. *Nano Lett.* **2011**, *11*, 4431-4437. https://doi.org/10.1021/nl2026426.

(2) Jourdan, M.; Minár, J.; Braun, J.; Kronenberg, A.; Chadov, S.; Balke, B.; Gloskovskii, A.; Kolbe, M.; Elmers, H. J.; Schönhense, G.; Ebert, H.; Felser, C.; Kläui, M. Direct observation of half-metallicity in the Heusler compound Co_2MnSi. *Nat. Commun.* **2014**, *5*, 3974. https://doi.org/10.1038/ncomms4974.

(3) Felser, C.; Wollmann, L.; Chadov, S.; Fecher, G. H.; Parkin, S. S. P. Basics and prospective of magnetic Heusler compounds. *APL Mater.* **2015**, *3*, 041518. https://doi.org/10.1063/1.4917387.

(4) Graf, T.; Felser, C.; Parkin, S. S. P. *Handbook of Spintronics* **2015**, 335, Springer Netherlands, ISBN: 978-940076892-5; 978-940076891-8.

(5) Idrissi, S.; Khalladi, R.; Ziti, S.; El Mekkaoui, N.; Mtougui, S.; Labrim, H.; El Housni, I.; Bahmad, L. The electronic and magnetic proprieties of the rare earth-based quaternary Heusler compound LuCoVGe. *Phys. B* **2019**, *562*, 116 -123. https://doi.org/10.1016/j.physb.2019.03.018.

(6) Li, H.; Li, X.; Kim, D.; Zhao, G.; Zhang, D.; Diao, Z.; Chen, T.; Wang, J.-P. High spin polarization in epitaxial Fe_4N thin films using Cr and Ag as buffer layers. *Appl. Phys. Lett*. **2018**, *112*, 162407. https://doi.org/10.1063/1.5023698.

(7) Graf, T.; Felser, C.; Parkin, S. S. P. Simple rules for the understanding of Heusler compounds. *Prog. Solid State Chem*. **2011**, *39*, 1-50. https://doi.org/10.1016/j.progsolidstchem.2011.02.001.

(8) Selinsky, R. S.; Keavney, D. J.; Bierman, M. J.; Jin, S. Element-specific magnetometry of EuS nanocrystals. *Appl. Phys. Lett*. **2009**, *95*, 202501. https://doi.org/10.1063/1.3251777.

(9) Bierman, M. J.; Van Heuvelen, K. M.; Schmeisser, D.; Brunold, T. C.; Jin, S. Ferromagnetic Semiconducting EuO Nanorods. *Adv. Mater*. **2007**, *19*, 2677-2681. https://doi.org/10.1002/adma.200602612.

(10) Dedkov, Yu. S.; Rüdiger, U.; Güntherodt, G. Evidence for the half-metallic ferromagnetic state of Fe_3O_4 by spin-resolved photoelectron spectroscopy. *Phys. Rev. B* **2002**, *65*, 064417. https://doi.org/10.1103/PhysRevB.65.064417.

(11) Kamper, K. P.; Schmitt, W.; Güntherodt, G.; Gambino, R. J.; Ruf, R. CrO_2-A New Half-Metallic Ferromagnet?. *Phys. Rev. Lett*. **1987**, *59*, 2788. https://doi.org/10.1103/PhysRevLett.59.2788.

(12) Hirohata, A.; Kikuchi, M.; Tezuka, N.; Inomata, K.; Claydon, J. S.; Xu, Y. B.; van der Laan, G. Heusler alloy/semiconductor hybrid structures. *Curr. Opin. Solid State Mater. Sci*. **2006**, *10*, 93-107. https://doi.org/10.1016/j.cossms.2006.11.006.

(13) Gercsi, Z.; Hono, K. Ab initio predictions for the effect of disorder and quarternary alloying on the half-metallic properties of selected Co_2Fe-based Heusler alloys. *J. Phys.: Condens. Matter* **2007**, 19, 326216. https://doi.org/10.1088/0953-8984/19/32/326216.

(14) Felser, C.; Hillebrands, B. New materials with high spin polarization: half-metallic Heusler compounds (Editorial). *J. Phys. D: Appl. Phys*. **2007**, *40*. https://doi.org/10.1088/0022-3727/40/6/E01.

(15) Obaida, M.; Galdun, L.; Ryba, T.; Komanicky, V.; Saksl, K.; Durisin, M.; Kovac, J. ; Haskova, V.; Szabo, P.; Vargova, Z.; Varga, R. Spin polarization in Cu_2MnSn Heusler alloy produced by melt-spinning. *Intermetallics* **2017**, *85*, 139-143. https://doi.org/10.1016/j.intermet.2017.02.014.

(16) Pogorily, A. N.; Kravets, A. F.; Nevdacha, V. V. ; Podyalovskiy, D. Y.; Ryabchenko, S. M.; Kalita, V. M.; Kulik, M. M.; Lozenko, A. F.; Vovk, A. Ya.; Godinho, M.; Maurel, L.; Pardo, J. A.; Magen, C.; Korenivski, V. Magnetic anisotropy of epitaxial Co_2Fe-Ge Heusler alloy films on MgO (100) substrates. *AIP Adv*. **2017**, *7*, 055831. https://doi.org/10.1063/1.4978209.

(17) Sahoo, R.; Das, A.; Stuesser, N.; Suresh, K. G. Field dependent neutron diffraction study in $Ni_{50}Mn_{38}Sb_{12}$ Heusler alloy. *Appl. Phys. Lett*. **2017**, *110*, 021902. https://doi.org/10.1063/1.4973921.

(18) Phatak, Ch.; Heinonen, O.; De Graef, M.; Petford-Long, A. Nanoscale Skyrmions in a Nonchiral Metallic Multiferroic: Ni_2MnGa. *Nano Lett*. **2016**, *16*, 4141-4148. https://doi.org/10.1021/acs.nanolett.6b01011.

(19) Shan, R.; Sukegawa, H.; Wang, W. H.; Kodzuka, M.; Furubayashi, T.; Ohkubo, T.; Mitani, S.; Inomata, K.; Hono, K. Demonstration of Half-Metallicity in Fermi-Level-Tuned Heusler Alloy $Co_2FeAl_{0.5}Si_{0.5}$ at Room Temperature. *Phys. Rev. Lett*. **2019**, *102*, 246601. https://doi.org/10.1103/PhysRevLett.102.246601.

(20) Sapkota, K. R.; Gyawali, P.; Forbes, A.; Pegg, I. L.; Philip, J. Synthesis and characterization of Co_2FeAl nanowires. *J. Appl. Phys*. **2012**, 111, 123906. https://doi.org/10.1063/1.4729807.

(21) Li, W.-J.; Khan, U.; Irfan, M.; Javed, K.; Liu, P.; Ban, S. L.; Han, X. F. Fabrication and magnetic investigations of highly uniform CoNiGa alloy nanowires. *J. Magn. Magn. Mater*. **2017**, *432*, 124-128. https://doi.org/10.1016/j.jmmm.2017.01.074.

(22) Hu, S.; Itoh, H.; Kimura, T. Efficient thermal spin injection using CoFeAl nanowire. *NPG Asia Mater*. **2014**, *6*, e127. https://doi.org/10.1038/am.2014.74.

(23) Simon, P.; Wolf, D.; Wang, Ch.; Levin, A. A.; Lubk, A.; Sturm, S.; Lichte, H.; Fecher, G. H.; Felser, C. Synthesis and Three-Dimensional Magnetic Field Mapping of Co_2FeGa Heusler Nanowires at 5 nm Resolution. *Nano Lett.* **2016**, *16*, 114-120. https://doi.org/10.1021/acs.nanolett.5b03102.

(24) Khan, S.; Ahmad, N.; Ahmed, N.; Safeer, A.; Iqbal, J.; Han, X. F. Structural, magnetic and transport properties of Fe-based full Heusler alloy Fe_2CoSn nanowires prepared by template-based electrodeposition. *J. Magn. Magn. Mater*. **2018**, *465*, 462-470. https://doi.org/10.1016/j.jmmm.2018.05.013.

(25) Khan, S.; Ahmad, N.; Ahmed, N.; Han, X. F. Analysis of electronic, magnetic and half-metallic properties of $L2_1$-type ($Co_2Mn_{0.5}Fe_{0.5}Sn$) Heusler alloy nanowires synthesized by AC-electrodeposition in AAO templates. *J. Magn. Magn. Mater*. **2018**, *460*, 120-127. https://doi.org/10.1016/j.jmmm.2018.03.028.

(26) Galdun, L.; Vega, V.; Vargova, Z.; Barriga-Castro, E. D.; Luna, C.; Varga, R.; Prida, V. M. Intermetallic Co_2FeIn Heusler Alloy Nanowires for Spintronics Applications. *ACS Appl. Nano Mater*. **2018**, *1*, 7066-7074. https://doi.org/10.1021/acsanm.8b01836.

(27) Safeer, A.; Ahmad, N.; Suleman, K.; Azam, L. A.; Bashir, D. Magnetization behavior of electrochemically synthesized Co_2MnSn full Heusler alloy nanowire arrays. *J. Appl. Phys*. **2019**, *125*, 034302. https://doi.org/10.1063/1.5058066.

(28) Xu, Y.; Yang, D.; Luo, Z.; Wu, F.; Chen, C.; Liu, M.; Yi, L.; Piao, H.-G.; Yu, G. Fabrication and magnetic properties of structure-tunable Co_2FeGa-SiO_2 Heusler nanocompounds. *AIP Adv*. **2018**, *8*, 055107. https://doi.org/10.1063/1.4986545.

(29) Sharma, M.; Das, A.; Kuanr, B. K. Co-based full heusler alloy nanowires: Modulation of static and dynamic properties through deposition parameters. *AIP Adv.* **2019**, *9*, 125054. https://doi.org/10.1063/1.5130036.

(30) Vemulkar, T.; Mansell, R.; Fernández-Pacheco, A.; Cowburn, R. P. Toward Flexible Spintronics: Perpendicularly Magnetized Synthetic Antiferromagnetic Thin Films and Nanowires on Polyimide Substrates. *Adv. Funct. Mater.* **2016**, *26*, 4704-4711. https://doi.org/10.1002/adfm.201505138.

(31) Parkin, S. S. P.; Hayashi, M.; Thomas, L. Magnetic Domain-Wall Racetrack Memory. *Science* **2008**, *320*, 190-194. https://doi.org/10.1126/science.1145799.

(32) Nazmunnahar, M.; Ryba, T.; del Val, J. J.; Ipatov, M.; González, J.; Hašková, V.; Szabó, P.; Samuely, P.; Kravcak, J.; Vargova, Z.; Varga, R. Half-metallic Ni_2MnSn Heusler alloy prepared by rapid quenching. *J. Magn. Magn. Mater*. **2015**, *386*, 98-101. https://doi.org/10.1016/j.jmmm.2015.03.066.

(33) Lehmann, H.; Scholtyssek, J. M.; Herrmann, C.; Herfort, J.; Merkt, U.; Meier, G. Point contact Andreev spectroscopy of epitaxial Co_2FeSi Heusler alloys on GaAs (001). *J. Appl. Phys.* **2011**, *110*, 063908. https://doi.org/10.1063/1.3632063.

(34) Makinistian, L.; Faiz, M. M.; Panguluri, R. P.; Balke, B.; Wurmehl, S.; Felser, C.; Albanesi, E. A.; Petukhov, A. G.; Nadgorny, B. On the half-metallicity of Co_2FeSi Heusler alloy: Point-contact Andreev reflection spectroscopy and ab initio study. *Phys. Rev. B.* **2013**, *87*, 220402(R). https://doi.org/10.1103/PhysRevB.87.220402.

(35) Huang, H.-L.; Tung, J-Ch.; Guo, G.-Y. Anomalous Hall effect and current spin polarization in Co_2FeX Heusler compounds (X=Al, Ga, In, Si, Ge, and Sn): A systematic ab initio study. *Phys. Rev. B.* **2015**, *91*, 134409. https://doi.org/10.1103/PhysRevB.91.134409.

(36) Duan, J.; Kou, X. Effect of Current Density on the Microstructure and Magnetic Properties of Electrodeposited Co_2FeSn Heusler Alloy. *J. Electrochem. Soc.* **2013**, *160*, D471. https://doi.org/10.1149/2.089310jes.

(37) Watanabe, N.; Sano, K.; Tasugi, N.; Yamaguchi, T.; Yamamoto, A.; Ueno, M.; Sumiyoshi, R.; Arakawa, T.; Koiwa, I. Preparation of Co_2FeSn Heusler alloys by electrodeposition method. *APL Mater.* **2015**, *3*, 041804. https://doi.org/10.1063/1.4918639.

(38) Lu, H.; Liu, Y.; Kou, X. Communication—Electrodeposition, Microstructure and Magnetic Properties of Co_2FeSn Heusler Alloy Nanowires. *J. Electrochem. Soc*. **2018**, *165*, D813. https://doi.org/10.1149/2.0751816jes.

(39) Wurmehl, S.; Alves, M. C. M.; Morais, J.; Ksenofontov, V.; Teixeira, S. R.; Machado, G.; Fecher, G. H.; Felser, C. Structural properties of the quaternary Heusler alloy $Co_2Cr_{1-x}Fe_xAl$. *J. Phys. D: Appl. Phys*. **2007**, *40*, 1524. https://doi.org/10.1088/0022-3727/40/6/S02.

(40) Miura, Y.; Nagao, K.; Shirai, M. Atomic disorder effects on half-metallicity of the full-Heusler alloys $Co_2(Cr1-xFe_x)Al$: A first-principles study. *Phys. Rev. B*, **2004**, *69*, 144413. https://doi.org/10.1103/PhysRevB.69.144413.

(41) Martínez Huerta, J.M.; De La Torre Medina, J.; Piraux, L.; Encinas, A. Self consistent measurement and removal of the dipolar interaction field in magnetic particle assemblies and the determination of their intrinsic switching field distribution. *J. Appl. Phys.*, **2012**, 111, 083914. https://doi.org/10.1063/1.4704397.

(42) Vega, V.; Böhnert, T.; Martens, S.; Waleczek, M.; Montero-Moreno, J.M., Görlitz, D.; Prida, V.M.; Nielsch, K. Tuning the magnetic anisotropy of Co–Ni nanowires: comparison between single

nanowires and nanowire arrays in hard-anodic aluminum oxide membranes. *Nanotechnology*, **2012**, 465709. https://doi.org/10.1088/0957-4484/23/46/465709.

(43) Sergelius, P.; Garcia Fernandez, J.; Martens, S.; Zocher, M.; Böhnert, T., Vega Martinez, V.; de la Prida, V. M.; Görlitz, D.; Nielsch, K. Statistical magnetometry on isolated NiCo nanowires and nanowire arrays: a comparative study. *J. Phys. D: Appl. Phys.*, **2016**, 49, 145005. https://doi.org/10.1088/0022-3727/49/14/145005.

(44) Fernandez-Roldan, J. A.; Perez del Real R.; Bran, C.; Vazquez, M.; Chubykalo-Fesenko, O. Magnetization pinning in modulated nanowires: from topological protection to the "corkscrew" mechanism. *Nanoscale*, **2018,** 10, 5923-5927. https://doi.org/10.1039/C8NR00024G.

(45) Plecenník, A.; Grajcar, M.; Beňačka, Š.; Seidel, P.; Pfuch, A. Finite-quasiparticle-lifetime effects in the differential conductance of $Bi_2Sr_2CaCu_2O_y$/Au junctions. *Phys. Rev. B* **1994**, *49*, 10016. https://doi.org/10.1103/PhysRevB.49.10016.

(46) Strijkers, G. J.; Ji, Y.; Yang, F. Y.; Chien, C. L.; Byers, J. M. Andreev reflections at metal/superconductor point contacts: Measurement and analysis. *Phys. Rev. B* **2001**, *63*, 104510. https://doi.org/10.1103/PhysRevB.63.104510.

(47) Clowes, S. K.; Miyoshi, Y.; Bugoslavsky, Y.; Branford, W. R.; Grigorescu, C.; Manea, S. A; Monnereau, O.; Cohen L. F. Spin polarization of the transport current at the free surface of bulk NiMnSb. *Phys. Rev. B* **2004,** 69, 214425. https://doi.org/10.1103/PhysRevB.69.214425

(48) Tanaka, M. A.; Ishikawa, Y.; Wada, Y.; Hori, S.; Murata, A.; Horii, S.; Yamanishi, Y.; Mibu, K.; Kondou, K.; Ono, T.; Kasai, S. Preparation of Co_2FeSn Heusler alloy films and magnetoresistance of Fe/MgO/Co_2FeSn magnetic tunnel junctions. *J. Appl. Phys.* **2012,** *111*, 053902. https://doi.org/10.1063/1.3688324.

(49) Varaprasad, B. S. D. Ch. S.; Srinivasan, A.; Takahashi, Y. K.; Hayashi, M.; Rajanikanth, A.; Hono, K. Spin polarization and Gilbert damping of $Co_2Fe(Ga_xGe_{1-x})$ Heusler alloys. *Acta Mater.* **2012**, *60*, 6257-6265. https://doi.org/10.1016/j.actamat.2012.07.045.

(50) Takahashi, Y. K.; Hono, K. **2016**, *Spin Polarization in Heusler Alloy Films*. In: Felser, C.; Hirohata A. (Eds.) Heusler Alloys. Springer Series in Materials Science, vol. 222, pp. 295-318. Springer, Cham., ISBN: 978-3-319-21449-8. https://doi.org/10.1007/978-3-319-21449-8_12.

(51) Zhao, Z.-S.; Xian, A.P. **2012,** *The Effect of Gelatin on the Tin Electrodeposition, 2012 13th International Conference on Electronic Packaging Technology & High Density Packaging, Guilin, pp. 521-524, doi: 10.1109/ICEPT-HDP.2012.6474672*

(52) Cullity, B. D.; Stock, S. R. **2001**, *Elements of X-ray Diffraction*, Third Edition. New York: Prentice-Hall.

Graphical Abstract:

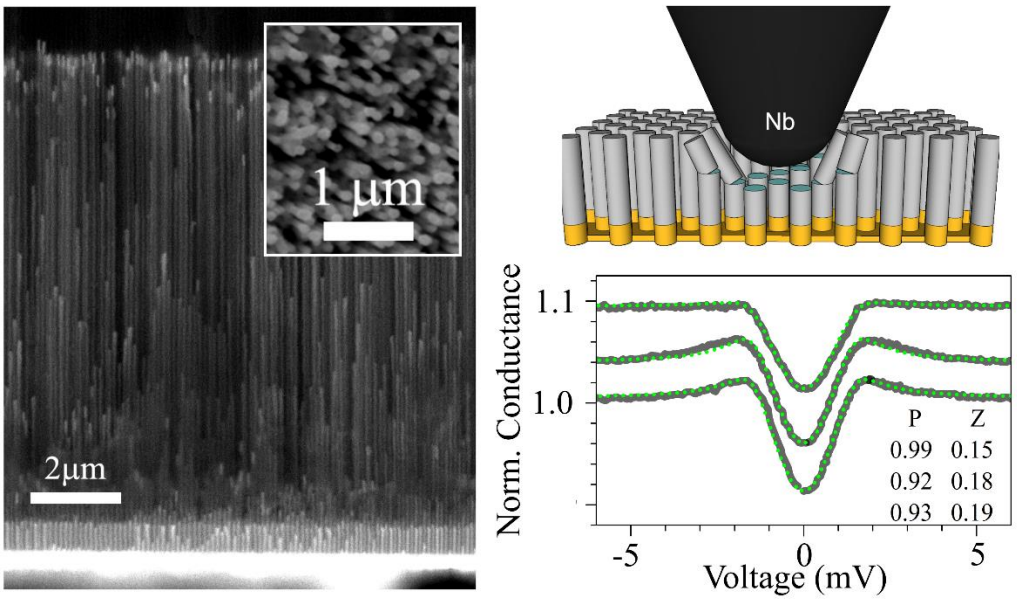

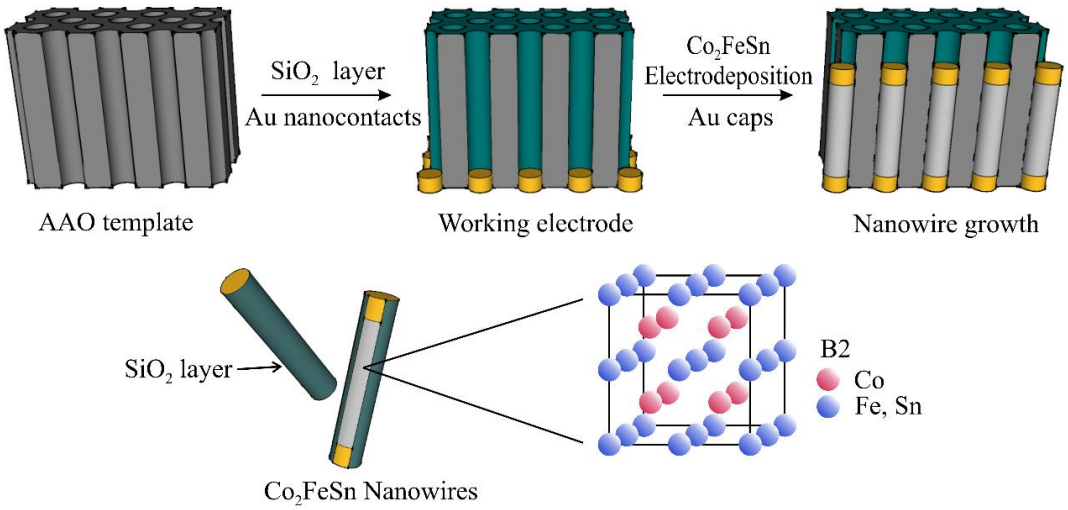
SiO2 layer
Au nanocontacts
Co2FeSn
Electrodeposition
Au caps
AAO template
Working electrode
Nanowire growth
SiO2 layer
Co2FeSn Nanowires
B2
Co
Fe, Sn

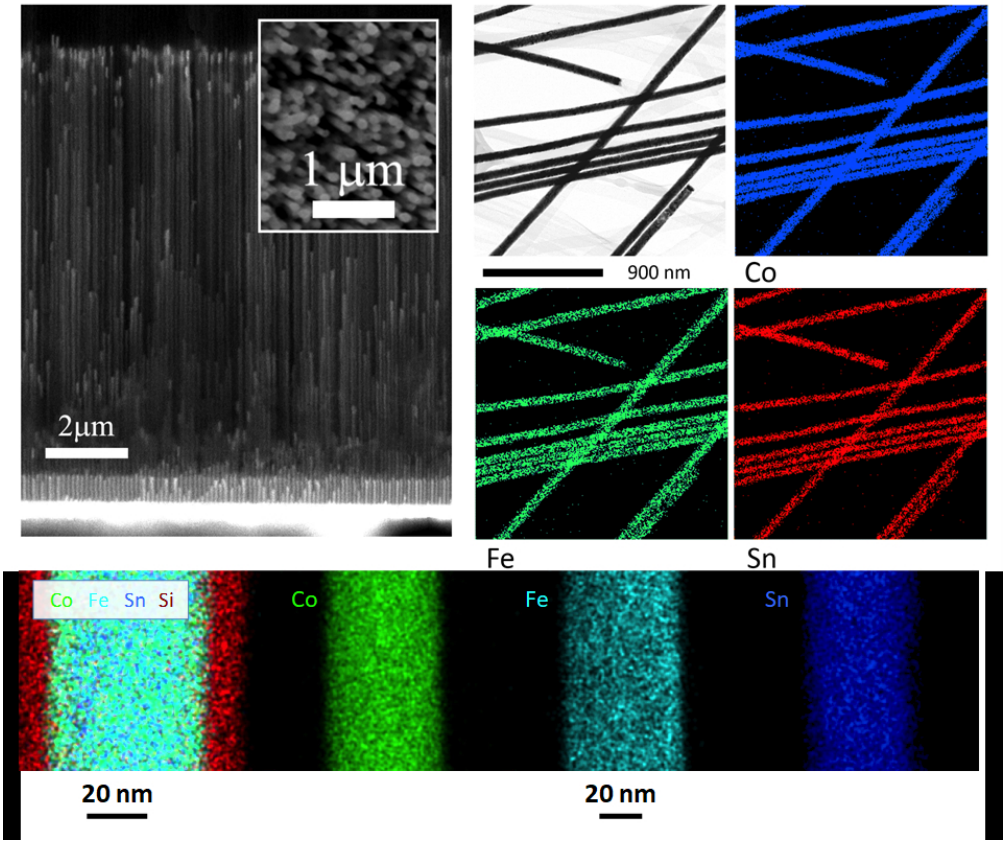

Figure 2. (left) the corresponding cross-section for the Co2FeSn nanowires in the array and SEM micrograph of the top view of free-standing nanowires without upper Au caps and protective SiO2 coating layer which is not present in the case of the sample prepared for microcontact spectroscopy (inset). (right, down) STEM analyses of Co2FeSn nanowires with EDS mapping disclose the uniform distribution of the atomic content of Co, Fe and Sn into the nanowires and the presence of the SiO2 coating layer.

253x215mm (96 x 96 DPI)

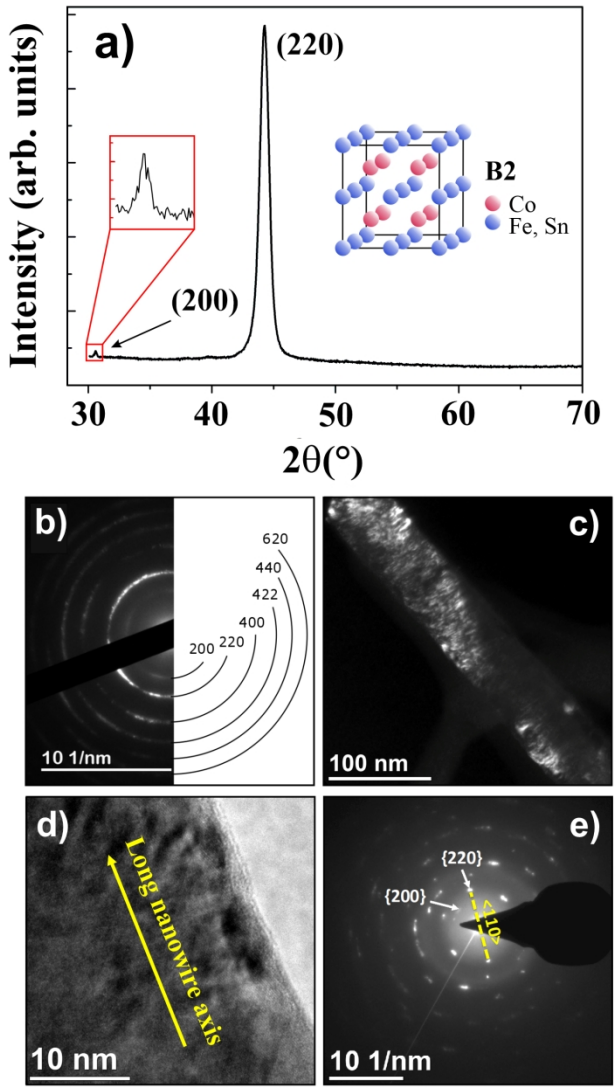

Figure 3. (a) XRD pattern of Co2FeSn nanowires electrodeposited into the alumina template with B2 cubic phase, (b) SAED pattern corresponding of several nanowires indexed to the B2-type cubic Co2FeSn Heusler structure. (c) Dark-field TEM image of a single nanowire. (d) HR-TEM micrograph of a single Co2FeSn nanowire, the arrow indicates the direction of the long axis of the nanowire, (e) SAED pattern of the same area studied in the panel (d). It is observed that the direction of the long nanowire axis, highlighted in panel (d), roughly falls in the <110> direction (see panel (e)).

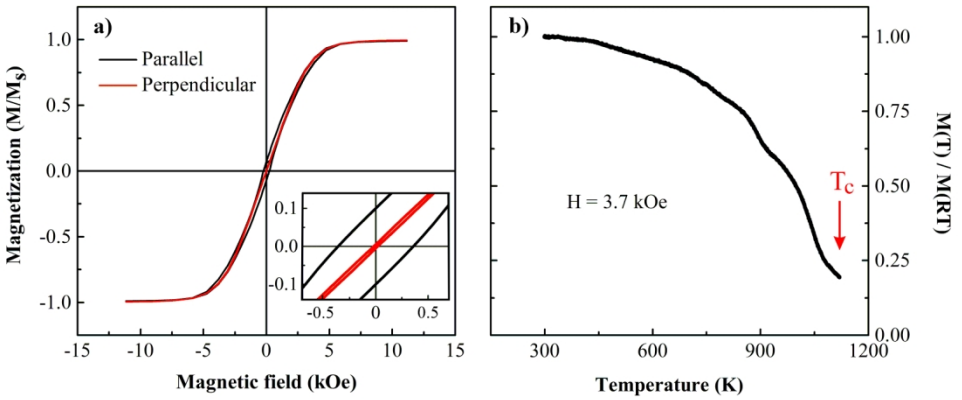

Figure 4. (a) Magnetic hysteresis loops measured at 300 K in an array of Co2FeSn nanowires for both the parallel and perpendicular direction with respect to the nanowire´s axis, (b) normalized temperature dependence of magnetization M(T)/M(RT), revealing high Curie temperature (>1000 K).

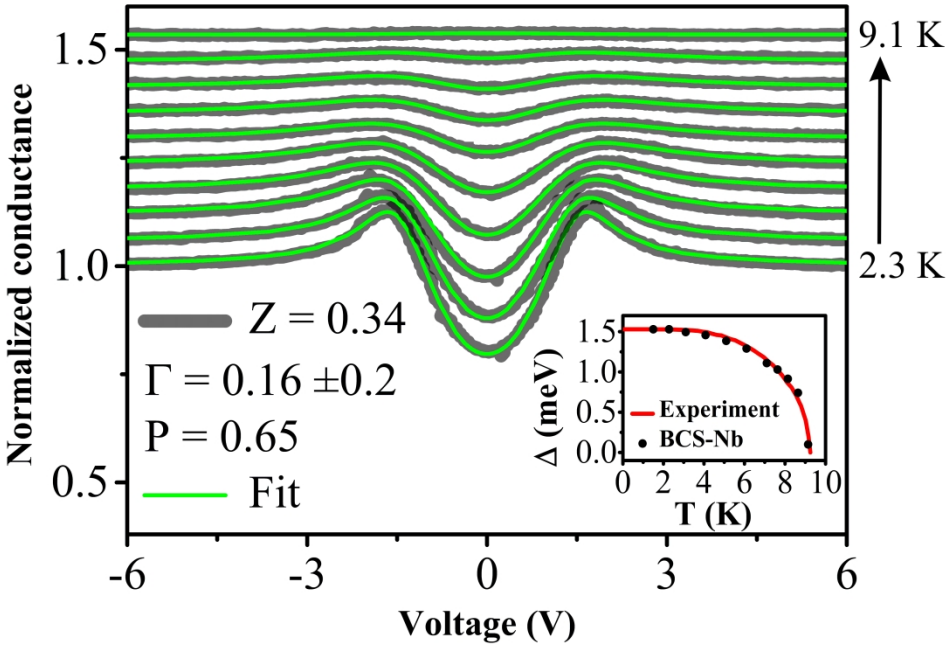

Figure 5. Temperature dependence of the Point-Contact Andreev Reflection spectra measured on an Nb/NW array point-contact at temperatures from the bottom curve 2.3 K, 3.1 K, 4.1 K, 5.1 K, 6.1 K, 7.1 K, 8.1 K, 8.6 K, and 9.1 K (gray symbols) and the corresponding fitting curves (green lines) and fitting parameters (see the legend). The inset shows the evolution of the superconducting energy gap of the Nb tip with temperature (black symbols) and predictions of the BCS theory (red line).

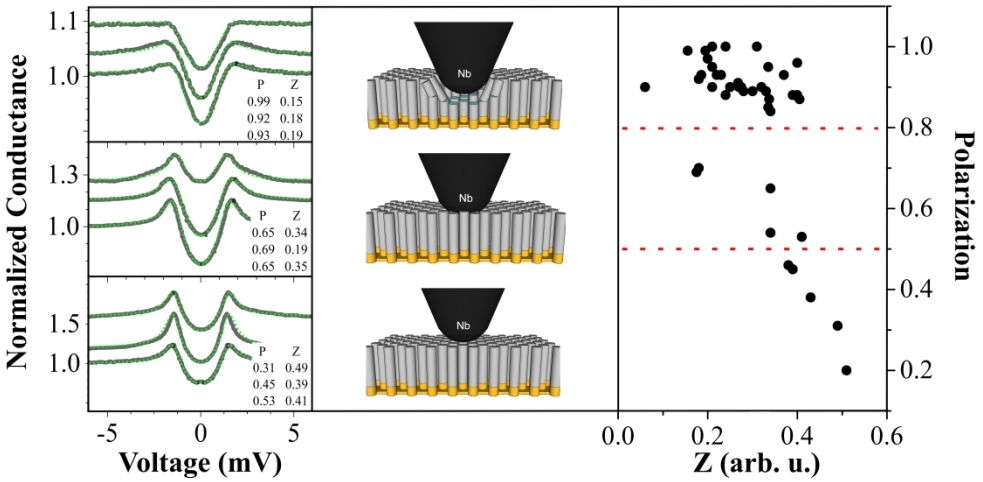

Figure 6. Spin polarization (P) dependence on barrier strength (Z) for Co2FeSn nanowire arrays - right panels and examples of PCAR experimental data (gray lines) and fits (green symbols) at T = 1.5 K in three different measuring modes – left panels. The values of spectral smearing parameter Γ were between Γ ~ 0.1Δ-0.5Δ. The results shown in the bottom and middle panels are characteristic for the point-contacts formed with weakly and strongly pressed Nb tip to NW array, respectively. The upper panels show results obtained on freshly cleaved NW array surfaces. The central 3D pictures visualize the point contact area in each mode.

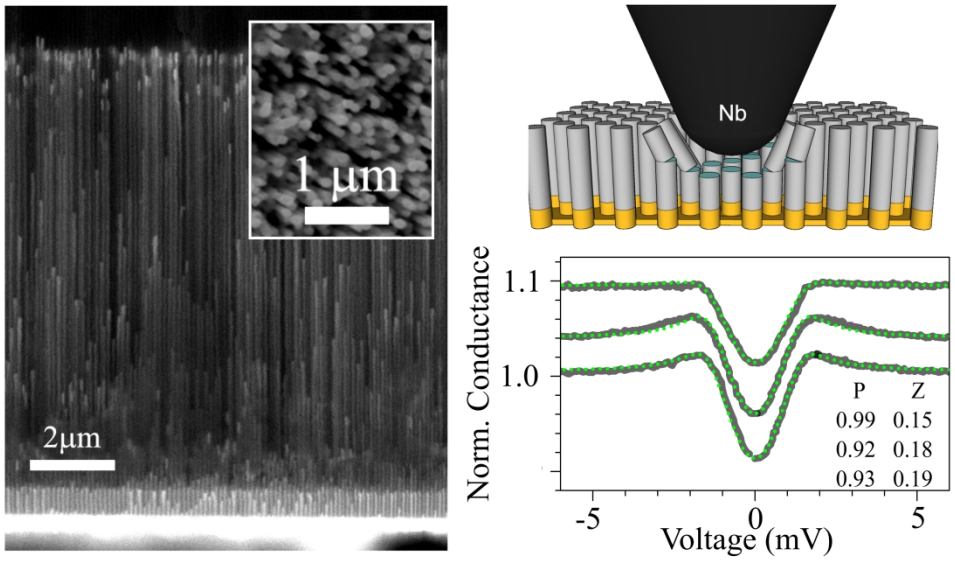

Graphical Abstract TOC